

## Article

# A Multi-Hook Control Strategy for a Semi-Active Device Combining an Adjustable Inerter and Damper

Xiaoliang Zhang<sup>1</sup>, Yimu Zhang<sup>1</sup>, Yue Zhao<sup>2</sup> and Jiamei Nie<sup>2,\*</sup> <sup>1</sup> Automotive Engineering Research Institute, Jiangsu University, Zhenjiang 212013, China<sup>2</sup> School of Automotive and Traffic Engineering, Jiangsu University, Zhenjiang 212013, China

\* Correspondence: niejm@ujs.edu.cn

**Abstract:** Neither the separate skyhook damping nor the skyhook inertance control strategy can adapt to the variations of both road and load conditions simultaneously. To address this issue, this work proposed a novel ideal multi-hook system by combining the skyhook inerter and hybrid damper, with both of their coefficients optimized. The proposed system can achieve road holding without sacrificing ride comfort. Depending on whether the inerter and damper were adjusted independently or together, this ideal multi-hook was realized semi-actively in two different control models with three different control strategies, i.e., independent, inertance-based and damping-based control. The effects of these strategies were compared and analyzed. The simulation results show that compared with passive suspension, the root mean square value of body acceleration of the three kinds of multi-hook suspension decreases by more than 40% under different loads and by more than 28% on the roads of Classes A, B and C. Compared with the skyhook damping suspension, the dynamic wheel load of the multi-hook suspensions is reduced by more than 27.5%, proving that the semi-active suspension system with multi-hook control guarantees handling stability under various road and load conditions while ensuring ride comfort.

**Keywords:** vehicle suspension; multi-hook; semi-active control; ride comfort; tire grounding



**Citation:** Zhang, X.; Zhang, Y.; Zhao, Y.; Nie, J. A Multi-Hook Control Strategy for a Semi-Active Device Combining an Adjustable Inerter and Damper. *Actuators* **2022**, *11*, 297. <https://doi.org/10.3390/act11100297>

Academic Editor: Hai Wang

Received: 31 August 2022

Accepted: 13 October 2022

Published: 16 October 2022

**Publisher's Note:** MDPI stays neutral with regard to jurisdictional claims in published maps and institutional affiliations.



**Copyright:** © 2022 by the authors. Licensee MDPI, Basel, Switzerland. This article is an open access article distributed under the terms and conditions of the Creative Commons Attribution (CC BY) license (<https://creativecommons.org/licenses/by/4.0/>).

## 1. Introduction

Being an essential part of vehicles, the suspension system plays a vital role in improving handling stability and ride comfort. Intensive studies on vehicle suspensions have driven their evolution from passive systems to semi-active or active ones. Passive suspension systems are simple and cheap [1–3], but they cannot be adapted to complex road conditions. Active suspension systems [4–6] use actuators instead of conventional springs and damping elements to control output forces online and are able to significantly improve vibration suppression, but high costs and energy consumption limit their widespread use in vehicle suspensions. Semi-active suspensions have become a hot topic in this research field because they can be considered as a compromise between passive and active suspension systems by varying the parameters of adjustable components to improve the suspension's performance [7,8] without consuming significant energy.

With the development of suspension systems, several semi-active control strategies have been proposed to meet the requirement for ride comfort. One classic control algorithm is the skyhook damping control strategy [9], which has been intensively studied since its appearance. Du et al. [10] proposed an adaptive skyhook control (ASC) based on an improved Genetic Algorithm (GA), which effectively reduced the vehicle body acceleration under different driving speeds. Ma et al. [11] designed an optimized fuzzy skyhook controller with a gray wolf optimizer (GWO) algorithm, with results showing that body acceleration was significantly reduced under different road conditions. Although the canopy damping control is effective in improving the ride comfort under varying road conditions and velocities, it does not consider the influence of vehicle load changes on

ride comfort, implying that it cannot realize dynamic tire load, thus reducing the handling stability [12].

Inerter was first introduced by Smith [13] in 2002 as a two-terminal element, in which the force applied to the two terminals is proportional to the relative acceleration between them. The scale factor is called the inertance coefficient and is measured in kilograms. In subsequent research, some scholars have applied inerter to vehicle suspensions, forming new suspension systems with damper and spring, i.e., the inerter–spring–damper (ISD) [14–17] suspension systems. Moreover, it has been found that the inerter can add fixed virtual mass to the sprung mass, thereby reducing the inherent frequency to improve ride comfort [18–20]. Nevertheless, a passive inerter is a non-active component whose inertance coefficients cannot be adjusted online, and it has limited ability in improving the vehicle suspension performance. As research progresses, semi-active inerters and control strategies have been gradually proposed, with the increasingly common use of semi-active inertance control in suspensions. Chen et al. [21,22] studied the application of adjustable inerters in semiactive suspensions and designed a semi-active inerter to illustrate the necessity and benefits of introducing semi-active inerters in suspensions. Wang [23] proposed a semi-active inerter control strategy for relative acceleration relative velocity control (RARV) and applied it to vehicle suspensions. Simulation results show that such a control strategy can achieve better performance indicators. Hu [24] presented a skyhook inertance control strategy which adds a virtual mass to the sprung mass to improve ride comfort. Zhang [25] combined skyhook inertance and the damping control strategy to propose three double-skyhook control strategies, and their results show that all three control strategies can enhance ride comfort, with the damping-based control strategy having the best performance.

While the double-skyhook control strategy guarantees riding comfort, it ignores the effect of dynamic tire load. The concept of groundhook damping control [26] is to install a damper between the ground reference and the unsprung mass, and its semi-active simulation results show that groundhook damping control can significantly suppress dynamic tire loads. In this paper, three semi-active control strategies are proposed to improve ride comfort and handling stability by combining the skyhook damping, skyhook inertance and groundhook damping controls. The proposed strategies are conducted with semi-active devices such as a damper or an inerter, or a combination thereof. The former is named as the independent multi-hook control (Ma), the latter is the combined multi-hook control, which can be further divided into the inertance-based (Mb) and damping-based (Mc) multi-hook controls according to whether the semi-active device is dominated by the inertance or damping. The results demonstrate that the combined control strategy can not only make the vehicle adapt to road and load conditions but also ensure appropriate handling stability.

The following content is organized as follows. In Section 2, the multi-hook configuration is introduced and the benefits of this configuration are qualitatively analyzed. In Section 3, two semi-active realizations of the multi-hook controls, including the independent multi-hook control and the combined multi-hook control, are investigated separately, and then three multi-hook control strategies are illustrated based on a quarter-car model. In Section 4, numerical simulations and analyses of the multi-hook control strategies are performed based on the verified model. Conclusions are drawn in Section 5.

## 2. Performance Benefits of the Multi-Hook System

A degree-of-freedom (DOF) model of the multi-hook system is shown in Figure 1, where  $m_2$  and  $m_1$  represent the sprung mass and unsprung mass, respectively.  $b_{sky}$  represents the inertance of the virtual inerter;  $c_{sky}$  and  $c_{gnd}$  are the damping coefficients of the virtual damper, in which *sky* means the damper is inserted between the stationary sky (the imaginary reference frame) and the sprung mass, while *gnd* means the damper is inserted between the stationary ground and the unsprung mass. A spring with the stiffness coefficient  $k$  and a damper with the damping coefficient  $c_b$  are settled between

the unsprung mass and sprung mass. The tire is modeled by a spring with the stiffness coefficient  $k_t$ . In this model,  $z_2$  (resp.,  $z_1$ ) is the vertical displacement of  $m_2$  (resp.,  $m_1$ ) and  $z_0$  is the road profile.

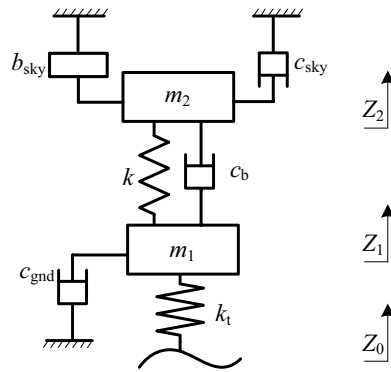


Figure 1. The 2DOF model of the multi-hook suspension system.

In the multi-hook configuration, the skyhook inerter is capable of simulating part of the sprung mass; the skyhook damper is used to suppress the vertical vibration of the body; and the groundhook damper is used to suppress the wheel runout. With the multi-hook system, the ride comfort is improved by reducing the acceleration and velocity of the sprung mass, and the handling stability is ensured by lowering the dynamic tire load. The skyhook damping force  $F_{sky\_c}$ , the skyhook inertance force  $F_{sky\_b}$  and the groundhook damping force  $F_{gnd\_c}$  can be expressed as:

$$\begin{cases} F_{sky\_b} = b_{sky}\ddot{z}_2 \\ F_{sky\_c} = c_{sky}\dot{z}_2 \\ F_{gnd\_c} = c_{gnd}\dot{z}_1 \end{cases} \quad (1)$$

The equations of motion for the multi-hook suspension system are as follows:

$$\begin{cases} m_2\ddot{z}_2 + b_{sky}\ddot{z}_2 + c_{sky}\dot{z}_2 + k(z_2 - z_1) + c_b(\dot{z}_2 - \dot{z}_1) = 0 \\ m_1\ddot{z}_1 + c_{gnd}\dot{z}_1 + c_b(\dot{z}_1 - \dot{z}_2) + k(z_1 - z_2) + k_t(z_1 - z_0) = 0 \end{cases} \quad (2)$$

where  $c_b(\dot{z}_2 - \dot{z}_1)$  is called the damping force of basic damper and is denoted by  $F_{base}$ .

### 2.1. Load Adaptation

Equation (2) can be rewritten as:

$$\begin{cases} (m_2 + b_{sky})\ddot{z}_2 + c_{sky}\dot{z}_2 + k(z_2 - z_1) + c_b(\dot{z}_2 - \dot{z}_1) = 0 \\ m_1\ddot{z}_1 + c_{gnd}\dot{z}_1 + c_b(\dot{z}_1 - \dot{z}_2) + k(z_1 - z_2) + k_t(z_1 - z_0) = 0 \end{cases} \quad (3)$$

where  $m_2 + b_{sky}$  is taken as a combined sprung mass, which is connected to a skyhook damper, as shown in Figure 2. This means  $b_{sky}$  can simulate part of the sprung mass, so it can be adjusted online according to Equation (4) to keep the system at a virtually full load at all times. In this way, even if the load condition changes, the system can always obtain the same performance at full-load conditions. These guarantee the multi-hook system to have good load adaptability. Thus, one has:

$$b_{sky} = m_f - m_2 \quad (4)$$

where  $m_f$  is the full-load mass.

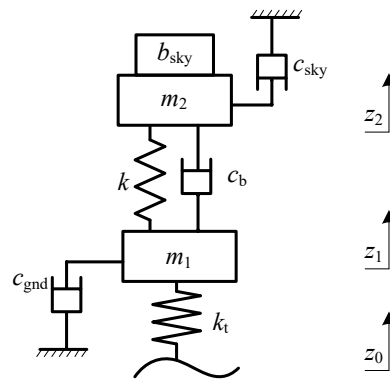


Figure 2. The equivalent system of the multi-hook suspension system.

### 2.2. Road Condition Adaptability

Under different road conditions, the skyhook damping needs to be adjusted online to ensure the suspension operation, so that the car can continuously obtain the ideal performance with excellent road adaptability. According to previous studies, the system damping ratio can be used as the control quantity [27,28], which can be calculated as:

$$\zeta = \frac{c_{sky} + c_b}{2\sqrt{(m_2 + b_{sky})k}} \tag{5}$$

Considering the requirements of ride comfort and handling stability, the system damping ratio should be controlled between the comfort damping ratio  $\zeta_c$  and the safety damping ratio  $\zeta_s$ , where the optimal damping ratio is determined [28].  $\zeta_c$  and  $\zeta_s$  are calculated by the following formula:

$$\zeta_c = \frac{1}{2} \sqrt{\frac{1 + \gamma_m}{\gamma_m \gamma_k}} \tag{6}$$

$$\zeta_s = \frac{1}{2} \sqrt{\frac{1 + \gamma_m}{\gamma_m \gamma_k} + \frac{\gamma_m \gamma_k - 2 - 2\gamma_m}{(1 + \gamma_m)^2}}, \tag{7}$$

respectively, where  $\gamma_k$  is the stiffness ratio and  $\gamma_m$  is the mass ratio, and they are expressed as

$$\gamma_k = \frac{k_t}{k} \tag{8}$$

and

$$\gamma_m = \frac{m_2 + b_{sky}}{m_1} \tag{9}$$

Based on Equation (1), the calculated  $c_{sky}$  can be used as the base damping  $c_{sum}$  for adjusting the skyhook and groundhook damping, then  $c_{sum}$  can be expressed by the following equation:

$$c_{sum} = c_{sky} = 2\zeta \sqrt{(m_2 + b_{sky})k} - c_b \tag{10}$$

As is shown in Equation (10), as road conditions change, the value of  $c_{sky}$  can be adjusted online according to the optimal damping ratio to adapt to this variation, verifying the adaptability of the system to road conditions.

### Optimization of the Multi-Hook Parameters under Different Road Conditions

Under different road conditions, vehicles have different requirements to realize dynamic performance. The damping ratios are selected for different road conditions

to regulate the  $c_{\text{sum}}$  and  $c_b$  online, so as to guarantee that the vehicle operates in the best state constantly.

Class A roads have better road conditions, so the driving speed on them is generally higher; therefore, the safety damping ratio is chosen to improve driving safety. On class C roads, the road conditions are poor with lower driving speed, so the damping ratio is chosen for comfort damping to improve driving smoothness. A comprehensive damping ratio was selected for class B roads. The obtained simulation conditions are given in Table 1.

**Table 1.** Vehicle speed and damping ratio under different road conditions.

Road Condition	Damping Ratio $\zeta$	Speed (m/s)
Class A	0.39	30
Class B	0.29	20
Class c	0.19	10

The objective function shown in Equation (11) transforms the multi-objective optimization problem into a single-objective optimization.

$$\min J = \frac{BA_s(z)}{BA_p} \alpha_1 + \frac{SWS_s(z)}{SWS_p} \alpha_2 + \frac{DTL_s(z)}{DTL_p} \alpha_3, \quad (11)$$

respectively, where  $BA_s(z)$ ,  $SWS_s(z)$  and  $DTL_s(z)$  are the root mean square (RMS) values of the body acceleration, suspension working space and dynamic tire load of the ideal multi-hook suspension system;  $BA_p$ ,  $SWS_p$  and  $DTL_p$  are the RMS of the corresponding performance indicators of the passive suspension under the same vehicle speed and road conditions. The weight coefficients  $\alpha_1$ ,  $\alpha_2$  and  $\alpha_3$  are determined from the variations of road conditions and vehicle speed as shown in Table 2, based on which, the coefficients  $c_{\text{sum}}$  and  $c_b$  were optimized for different road classes using a genetic algorithm, and the results are shown in Table 3.

**Table 2.** Weight coefficient distribution under different road conditions.

Road Condition	$\alpha_1$	$\alpha_2$	$\alpha_3$
Class A	0.7	0.15	0.15
Class B	0.4	0.2	0.4
Class c	0.15	0.15	0.7

**Table 3.** Optimized parameter results.

Road Condition	$c_{\text{sum}} (\text{N} \cdot \text{s} \cdot \text{m}^{-1})$	$c_b (\text{N} \cdot \text{s} \cdot \text{m}^{-1})$
Class A	1067	4700
Class B	1818	3550
Class c	2521	2450

### 2.3. Handling Stability

The skyhook damping control strategy is widely used in conventional semi-active suspension systems, but it inevitably leads to the deterioration of handling stability. Consequently, based on the introduction of skyhook damping and inertance, the structure of groundhook damping is added to reduce the vibration of unsprung mass by providing a reverse force that is proportional to its absolute velocity. In this way, the handling stability is improved. The grounded damping force can be calculated by

$$F_d = -c_{\text{gnd}} \dot{z}_1 \quad (12)$$

One limitation is that the multi-hook system described above is only an ideal configuration. It is not feasible to connect the damper and inerter to the static reference frame. Hence, the realization of control systems should be implemented via a semi-active or active actuator.

### 3. Semi-Active Realization of the Multi-Hook Control

In this section, two semi-active implementation methods of multi-hook control systems are proposed: one adopts an adjustable damper and an adjustable inverter, which are independent of each other, as shown in Figure 3a, and another adopts a semi-active device combining an adjustable damper and inverter, as shown in Figure 3b.

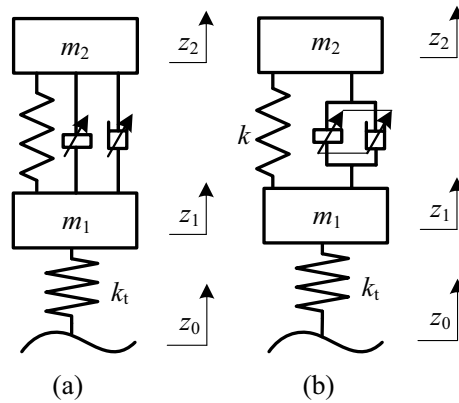


**Figure 3.** Two semi-active implementations of the multi-hook control systems: (a) semi-active suspension with an adjustable inverter and an adjustable damper; (b) semi-active suspension with a semi-active device of combining an adjustable inverter and damper.

The equations of motion of the semi-active suspensions shown in Figure 3 can be expressed as:

$$\begin{cases} m_2\ddot{z}_2 + k(z_2 - z_1) + [B(x)(\ddot{z}_2 - \ddot{z}_1) + C(x)(\dot{z}_2 - \dot{z}_1)] = 0 \\ m_1\ddot{z}_1 - k(z_2 - z_1) - [B(x)(\ddot{z}_2 - \ddot{z}_1) + C(x)(\dot{z}_2 - \dot{z}_1)] + k_t(z_1 - z_0) = 0 \end{cases} \quad (13)$$

where  $B(x)$  and  $C(x)$  are the inverter and the damping coefficients, respectively, and  $x$  is control variable.  $B(x)(\ddot{z}_2 - \ddot{z}_1)$  and  $C(x)(\dot{z}_2 - \dot{z}_1)$  are the forces provided by the inverter and damper, respectively, which are marked as  $F_b$  and  $F_c$ , respectively.

It should be noted that there are differences between the semi-active suspension and ideal multi-hook system, so two coefficients, i.e.,  $k_1$  and  $k_2$ , are introduced to make the multi-hook control strategy better adapted to the changes in road conditions. The adjustable inverter force  $F_b'$  and the adjustable damping force  $F_c'$  can be calculated as

$$\begin{cases} F_b' = -b_{sky}\ddot{z}_2 \\ F_c' = -\beta k_1 c_{sum}\sigma_{sky} + (1 - \beta)k_2 c_{sum}\sigma_{gnd} - c_b(\dot{z}_2 - \dot{z}_1) \end{cases} \quad (14)$$

where

$$\sigma_{sky} = \begin{cases} \dot{z}_2 & \dot{z}_2(\dot{z}_2 - \dot{z}_1) > 0 \\ 0 & \dot{z}_2(\dot{z}_2 - \dot{z}_1) \leq 0 \end{cases}$$

$$\sigma_{gnd} = \begin{cases} \dot{z}_1 & \dot{z}_1(\dot{z}_1 - \dot{z}_2) > 0 \\ 0 & \dot{z}_1(\dot{z}_1 - \dot{z}_2) \leq 0 \end{cases}$$

where  $\beta$  is the damping distribution coefficient, which ranges from 0 to 1. It represents the proportion of the skyhook damping in the sum of the skyhook and groundhook damping  $c_{sum}$ . When  $\beta = 0$ , there is only the groundhook damping; when  $\beta = 1$ , only skyhook damping is controlled. Considering that an appropriate increase in the proportion of the groundhook damping is beneficial to restrain the tire vibration,  $\beta$  is set as 0.3 in this paper.

In Figure 3a,  $F_b$  and  $F_c$  should be, respectively, equal to  $F_b'$  and  $F_c'$  to realize the ideal structure. That is

$$\begin{cases} B(x)(\ddot{z}_2 - \ddot{z}_1) = b_{sky}\ddot{z}_2 \\ C(x)(\dot{z}_2 - \dot{z}_1) = \beta k_1 c_{sum}\sigma_{sky} - (1 - \beta)k_2 c_{sum}\sigma_{gnd} + c_b(\dot{z}_2 - \dot{z}_1) \end{cases} \quad (15)$$

For the configuration in Figure 3b, the resultant forces of  $F_b$  and  $F_c$  are set equal to those of  $F'_b$  and  $F'_c$ .

$$B(x)(\ddot{z}_2 - \ddot{z}_1) + c(x)(\dot{z}_2 - \dot{z}_1) = b_{sky}\ddot{z}_2 + \beta k_1 c_{sum}\sigma_{sky} - (1 - \beta)k_2 c_{sum}\sigma_{gnd} + c_b(\dot{z}_2 - \dot{z}_1) \tag{16}$$

Based on this classification, two control strategies of multi-hook control can be given in Sections 3.2 and 3.3.

### 3.1. Optimization of the Damping Gain Factor

As the dynamic tire load inevitably deteriorates during the semi-active realization of the skyhook damping,  $k_1, k_2$  are optimized for different road conditions by using the MATLAB genetic algorithm toolbox with tire grounding as the optimization objective, and the optimization results are shown in Table 4.

**Table 4.** Optimization results of damping gain coefficient.

Control Strategies	Damping Ratio $\zeta$	Gain Coefficient $k_1$	Gain Coefficient $k_2$
multi-hook Ma	0.19	1	0.1
	0.29	1.9	0.1
	0.39	0.1	0.1
multi-hook Mb	0.19	1.3	0.1
	0.29	2.5	0.1
	0.39	0.1	0.1
multi-hook Mc	0.19	1.3	0.6
	0.29	1.9	0.7
	0.39	0.1	0.5

### 3.2. Independent Multi-Hook Control

Equation (15) can be rewritten as

$$\begin{cases} B(x) = \frac{b_{sky}\ddot{z}_2}{\ddot{z}_2 - \ddot{z}_1} \\ C(x) = \frac{\beta k_1 c_{sum}\sigma_{sky} - (1 - \beta)k_2 c_{sum}\sigma_{gnd} + c_b(\dot{z}_2 - \dot{z}_1)}{\dot{z}_2 - \dot{z}_1} \end{cases} \tag{17}$$

Considering the limitations of the actual device, the control laws of the independent semi-active inerter and damper can be obtained as

$$B(x) = \begin{cases} B_{min}, & \ddot{z}_2(\ddot{z}_2 - \ddot{z}_1) \leq 0; \\ \max\left(B_{min}, \min\left(\frac{b_{sky}\ddot{z}_2}{\ddot{z}_2 - \ddot{z}_1}, B_{max}\right)\right), & \ddot{z}_2(\ddot{z}_2 - \ddot{z}_1) > 0. \end{cases} \tag{18}$$

$$C(x) = \begin{cases} C_{min}, & \dot{z}_2(\dot{z}_2 - \dot{z}_1) \leq 0; \\ \max(C_{min}, \min(C_i, C_{max})), & \dot{z}_2(\dot{z}_2 - \dot{z}_1) > 0, \end{cases} \tag{19}$$

respectively, where

$$C_i = \frac{\beta k_1 c_{sum}\sigma_{sky} - (1 - \beta)k_2 c_{sum}\sigma_{gnd} + c_b(\dot{z}_2 - \dot{z}_1)}{\dot{z}_2 - \dot{z}_1}$$

The underlining idea of the skyhook inertance control law [24] Equation (18) is to make the  $B(x)$  transfer  $b_{sky}\ddot{z}_2/(\ddot{z}_2 - \ddot{z}_1)$  when the semi-active force has the same direction as the skyhook inerter force and transmit the minimal force when the directions are reversed.  $B_{min}$  and  $B_{max}$  indicate the maximum and minimum inertance coefficients that can be provided by the semi-active inerter. The idea of the skyhook damping control law Equation (19) is to

make the  $C(x)$  transfer  $C_i$  when the velocity of the sprung mass is in the same direction as the relative velocity, taking the minimum damping force when the directions are opposite.  $C_{\min}$  and  $C_{\max}$  indicate the maximum and minimum damping coefficients that can be provided by the semi-active damper.

### 3.3. Combined Multi-Hook Control

The combined control strategy is implemented by a verified semi-active device designed by our group and verified experimentally, which is characterized by its ability to provide both damping and inertial forces, and whose damping and inertance coefficients are both functions about its spool displacement  $x$ . There exists a ratio relationship between the damping and inertance coefficients [25], that is

$$C(x) = \alpha B(x) \tag{20}$$

where  $\alpha$  is the damping–inertance ratio of the device.

When the coefficient of damping is used as the control variable, it is referred to as the damping-based multi-hook control. When the inertance coefficient is used as the control variable, it is referred to as the inertance-based multi-hook control. According to Equations (16) and (20), the inertance-based multi-hook control law is:

$$B(x) = \begin{cases} B_{\min}, & \dot{z}_2(\dot{z}_2 - \dot{z}_1) \leq 0; \\ \max(B_{\min}, \min(B_c, B_{\max})), & \dot{z}_2(\dot{z}_2 - \dot{z}_1) > 0. \end{cases} \tag{21}$$

in which

$$B_c = \frac{\beta k_1 c_{\text{sum}} \sigma_{\text{sky}} - (1 - \beta) k_2 c_{\text{sum}} \sigma_{\text{gnd}} + c_b(\dot{z}_2 - \dot{z}_1) + b_{\text{sky}} \ddot{z}_2}{\ddot{z}_2 - \ddot{z}_1 + \alpha(\dot{z}_2 - \dot{z}_1)}$$

The damping-based multi-hook control law is:

$$C(x) = \begin{cases} C_{\min}, & \dot{z}_2(\dot{z}_2 - \dot{z}_1) \leq 0; \\ \max(C_{\min}, \min(C_c, C_{\max})), & \dot{z}_2(\dot{z}_2 - \dot{z}_1) > 0, \end{cases} \tag{22}$$

respectively, where

$$C_c = \frac{\beta k_1 c_{\text{sum}} \sigma_{\text{sky}} - (1 - \beta) k_2 c_{\text{sum}} \sigma_{\text{gnd}} + c_b(\dot{z}_2 - \dot{z}_1) + b_{\text{sky}} \ddot{z}_2}{\frac{\ddot{z}_2 - \ddot{z}_1}{\alpha} + \dot{z}_2 - \dot{z}_1}$$

## 4. Simulation and Analysis of Multi-Hook Control Strategies

This section verifies the effectiveness of the proposed multi-hook control strategy by simulation. A light truck is chosen in this simulation, and the parameters of its quarter vehicle model are provided in Table 5.

**Table 5.** Model parameters of the quarter vehicle.

Description	Value	Unit
Unsprung mass $m_1$	122.5	kg
Sprung mass (no load) $m_2$	500	kg
Sprung mass (full load) $m_2$	1100	kg
Suspension stiffness coefficient $k$	77.9	kN m <sup>-1</sup>
Tire stiffness coefficient $k_t$	584	kN m <sup>-1</sup>

### 4.1. Analysis of Load Adaptability

In this subsection, the performances of passive suspensions and these semi-active suspensions are compared under different loads to verify if semi-active suspensions with multi-hook control are able to adapt to load change as an ideal virtual multi-hook system.

For the passive suspension, the sprung mass is given as 500 kg, 800 kg and 1100 kg at the conditions of no load, half load and full load, respectively. For semi-active suspensions, the corresponding skyhook inertances  $b_{sky}$  are set to 600 kg, 300 kg and 0 kg to keep the suspensions at a virtual full-load condition. To simplify presentation, the independent, inertance-based and damping-based multi-hook control are referred to as Ma, Mb and Mc, respectively, in the following.

4.1.1. Frequency Responses to Sinusoidal Excitations

To investigate the performance of the three types of suspensions with multi-hook control strategies under different loads, all damping ratios were set to  $\zeta = 0.29$ . A sine wave  $z_0 = A\sin(2\pi ft)$  was used as the excitation, where  $f$  ranged from 1 Hz to 100 Hz and  $A = 0.1 \text{ m s}^{-1}$ . Figure 4 compares the RMS of BA for the passive suspension and the semi-active suspensions with multi-hook control strategies at each frequency. The resonant frequencies and the corresponding peak values for each suspension are listed in Table 6.

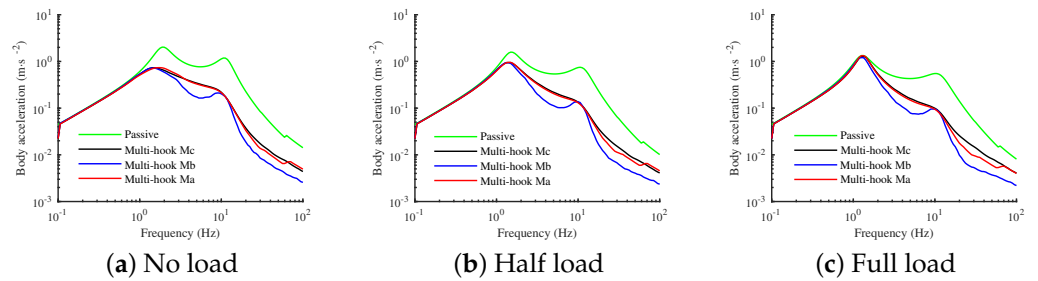


Figure 4. Comparison of body acceleration RMS values between the passive suspension and the semi-active suspensions with the multi-hook controls under different loads.

Table 6. Resonant frequencies and peak RMS values of body acceleration for the passive suspension and the semi-active suspensions with the double-skyhook controls under different loads.

Load	Indexes	Passive	Ma	Decline (%)	Mb	Decline (%)	Mc	Decline (%)
No load	Low frequency f1 (Hz)	1.88	1.78	5.6	1.41	25.0	1.41	25.0
	Peak value P1 ( $\text{m s}^{-2}$ )	2.03	0.74	63.7	0.72	64.4	0.73	63.9
	High frequency f1 (Hz)	10.59	10.00	5.9	9.44	10.8	10.00	5.9
	Peak value P2 ( $\text{m s}^{-2}$ )	1.18	0.21	81.8	0.21	82.2	0.22	81.6
Half load	Low frequency f1 (Hz)	1.50	1.41	5.5	1.41	5.5	1.41	5.5
	Peak value P1 ( $\text{m s}^{-2}$ )	1.58	0.95	39.8	0.94	40.8	0.95	40.2
	High frequency f1 (Hz)	10.00	10.00	0.0	10.00	0.0	10.00	0.0
	Peak value P2 ( $\text{m s}^{-2}$ )	0.75	0.12	83.9	0.14	81.8	0.13	82.1
Full load	Low frequency f1 (Hz)	1.33	1.33	0.0	1.33	0.0	1.33	0.0
	Peak value P1 ( $\text{m s}^{-2}$ )	1.34	1.33	0.8	1.21	9.8	1.27	4.8
	High frequency f1 (Hz)	10.00	10.00	0.0	9.44	5.6	10.00	0.0
	Peak value P2 ( $\text{m s}^{-2}$ )	0.55	0.09	82.8	0.096	82.6	0.10	81.9

As seen from Table 6, load change has a quite limited effect on the resonant frequency of the unsprung mass for all suspensions, but it mainly affects that of the sprung mass. Furthermore, it can be observed that the variation in the resonant frequency of the sprung mass for the multi-hook semi-active suspension is smaller than for the passive suspension as the load varies, and, in particular, the variations in Mb and Mc for the multi-hook semi-active suspension are extremely slight. In addition to this, Table 6 indicates that the spring mass resonance frequencies of the semi-active suspension under full load are the same as those of the passive suspension. Seeing from this perspective, the multi-hook control can enable the suspension to approach the suspension performance of the vehicle

at full load under different load conditions, which explains why it has the same sprung mass resonance frequency.

On the other hand, the peak RMS values for the semi-active suspension are significantly reduced at low frequencies (resonant frequencies of the sprung mass) and high frequencies (resonant frequencies of the unsprung mass) under all load conditions compared with the passive suspension, as show in Table 6. Figure 4 shows that the RMS values of acceleration are reduced across the entire frequency range for all load conditions, which implies that the multi-hook control is capable of simulating full-load conditions and significantly improving ride comfort.

#### 4.1.2. Time Responses to a Random Excitation

On real roads, the response to a random excitation simulates the vehicle. The filtered white noise signal is used as the road input model, that is

$$\dot{z}_0 = -2\pi n_1 v z_0(t) + 2\pi \sqrt{G_0 v} w(t), \tag{23}$$

where  $z_0(t)$  is road displacement in  $m$ ;  $G_0$  is road roughness coefficient in  $64 \times 10^{-6} \text{ m}^3 \text{ cycle}^{-1}$ , which is assumed to be a class B road in this study. The target vehicle speed  $v$  is set at  $20 \text{ m s}^{-1}$ ;  $w(t)$  is zero-mean Gaussian white noise with intensity 1, and  $n_1$  is low cut-off frequency, which is assumed to be a  $0.01 \text{ cycle m}^{-1}$ .

Figure 5 and Table 7 compare the time domain response of the suspension body acceleration under each load. As can be seen, the ride smoothness of the semi-active suspension using the hybrid shed control is better under all load conditions compared with the passive suspension, especially for the hybrid sheds Mb and Mc.

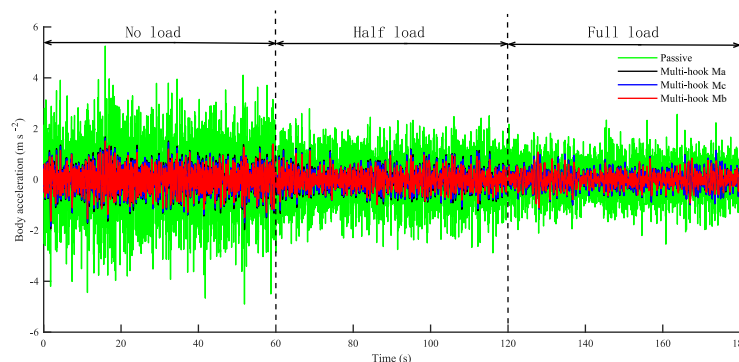


Figure 5. Time response comparison of body acceleration under different loads.

Table 7. RMS values of body acceleration for time response to a random excitation under different loads.

Load	Passive		Ma		Mb		Mc	
	RMS ( $\text{m s}^{-2}$ )	RMS ( $\text{m s}^{-2}$ )	Decline (%)	RMS ( $\text{m s}^{-2}$ )	Decline (%)	RMS ( $\text{m s}^{-2}$ )	Decline (%)	
No load	1.25	0.45	64.0	0.36	71.2	0.42	66.4	
Half load	0.86	0.40	53.5	0.32	62.8	0.38	55.8	
Full load	0.67	0.37	44.8	0.32	52.2	0.38	43.3	

The RMS values for the BA of the multi-hook semi-active suspension under all loads are less than those for the passive suspension under full load, as seen in Table 7. When the vehicle is unloaded, the RMS values of BA increase from  $0.67 \text{ m s}^{-2}$  to  $1.25 \text{ m s}^{-2}$  for the passive suspension and from  $0.37 \text{ m s}^{-2}$  to  $0.45 \text{ m s}^{-2}$ , from  $0.30 \text{ m s}^{-2}$  to  $0.36 \text{ m s}^{-2}$  and from  $0.38 \text{ m s}^{-2}$  to  $0.42 \text{ m s}^{-2}$  for the multi-hook controls Ma, Mb and Mc, respectively. This means that from full- to no-load, the RMS value of BA for multi-hook control changes less and adapts better to load changes.

#### 4.2. Analysis of Road Condition Adaptability

During simulation, the passive suspension is set to full load. The damping ratio  $\zeta$  of the passive suspension is set to 0.29 in this paper. The multi-hook semi-active suspension is set to no load, as the semi-active suspension can simulate the full-load condition through canopy inertia control.

The filtered white noise signal shown in Equation (23) is also used here as the road input model, where the road roughness coefficients  $G_0$  are  $16 \times 10^{-6} \text{ m}^3 \text{ cycle}^{-1}$  for road class A,  $64 \times 10^{-6} \text{ m}^3 \text{ cycle}^{-1}$  for road class B and  $256 \times 10^{-6} \text{ m}^3 \text{ cycle}^{-1}$  for road class C, which represent good, average and poor roads, respectively. For comparison purposes, the simulation results for BA under each road condition are placed on the same time domain plot, as shown in Figure 6. The RMS values for BA are listed in Table 8.

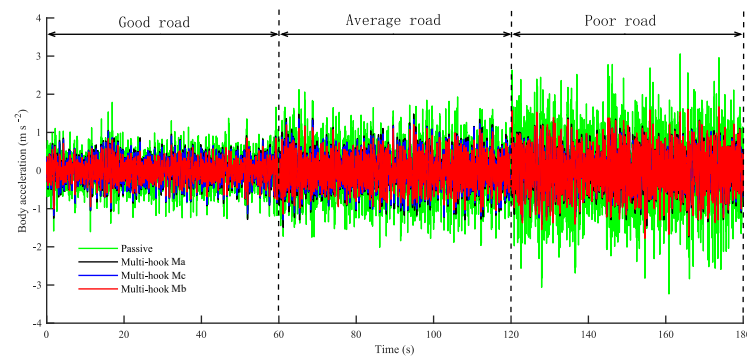


**Figure 6.** Time response comparison of body acceleration under different road conditions.

**Table 8.** RMS values of body acceleration for time response to a random excitation under different road conditions.

Road	Passive	Ma		Mb		Mc	
	RMS ( $\text{m s}^{-2}$ )	RMS ( $\text{m s}^{-2}$ )	Decline (%)	RMS ( $\text{m s}^{-2}$ )	Decline (%)	RMS ( $\text{m s}^{-2}$ )	Decline (%)
Class A	0.39	0.28	28.2	0.21	46.2	0.27	30.8
Class B	0.64	0.45	29.7	0.36	43.8	0.42	34.4
Class C	0.91	0.53	41.8	0.54	40.7	0.49	46.2

As observed from Figure 6, compared with the passive suspension, the semi-active suspensions with the multi-hook control resulted in significant decline in BA under all road conditions, particularly for the multi-hook controls Mb and Mc. These results show that the multi-hook controls are able to offer a high level of ride comfort under different road conditions.

Furthermore, as can be seen from Table 8, when the vehicle travels from a road with good conditions to a poor one, the RMS values of BA increase from  $0.39 \text{ m s}^{-2}$  to  $0.91 \text{ m s}^{-2}$  for the passive suspension and from  $0.28 \text{ m s}^{-2}$  to  $0.53 \text{ m s}^{-2}$ , from  $0.21 \text{ m s}^{-2}$  to  $0.54 \text{ m s}^{-2}$  and from  $0.27 \text{ m s}^{-2}$  to  $0.49 \text{ m s}^{-2}$  for Ma, Mb and Mc, respectively. According to these data, the RMS value variations (max, minus and min) of Ma, Mb and Mc are 51.9%, 36.5% and 57.7% lower than those of the passive suspension, respectively, when road conditions changed from good to bad. This demonstrates that the multi-hook control strategy can adapt to changes in road conditions and provide stable driving comfort, as changes in road conditions have less impact on BA and its RMS value.

#### 4.3. Comparative Analysis of Single-Skyhook and Multi-Hook Control Strategies

Notably, the skyhook damping control, despite being able to enhance road adaptability, can exacerbate vibrations in unsprung masses, which means it can deteriorate an important indicator of road holding, i.e., dynamic tire loads. To investigate the effect of groundhook damping in the multi-hook control strategy in reducing dynamic tire load, this

subsection compares the performance between single-skyhook suspensions and multi-hook suspensions. All suspensions were set to no-load conditions to better represent the effect of skyhook inertance on suspension performance.

#### 4.3.1. Time Response Analysis

For simulation, the same signals in Section 4.2 were used as inputs for the road inputs, and all the suspensions were set to no-load. The outputs are the BA and the time domain response of the DTL of each suspension, as shown in Figures 7–9. The total RMS values for each suspension indicator are shown in Table 9. It is clear that the multi-hook-controlled suspension outperforms the single-canopy suspension and the passive suspension. The simulation results show that the multi-hook suspension effectively improves ride smoothness and tire holding. Nevertheless, due to the trade-off between smoothness and safety performance, the operational stability of the inerter-based multi-hook control is slightly worse than that of the skyhook inertance control, but it is still within acceptable limits.

**Table 9.** Total RMS values under different road conditions for time response

Index	Passive	Skyhook Inertance	Skyhook Damp Ing	Ma	Mb	Mc
BA ( $m\ s^{-2}$ )	1.29	1.24	1.03	0.42	0.38	0.40
SWS (mm)	4.73	4.68	5.41	4.13	4.60	4.30
DTL (kN)	1.33	1.36	1.89	1.30	1.37	1.31

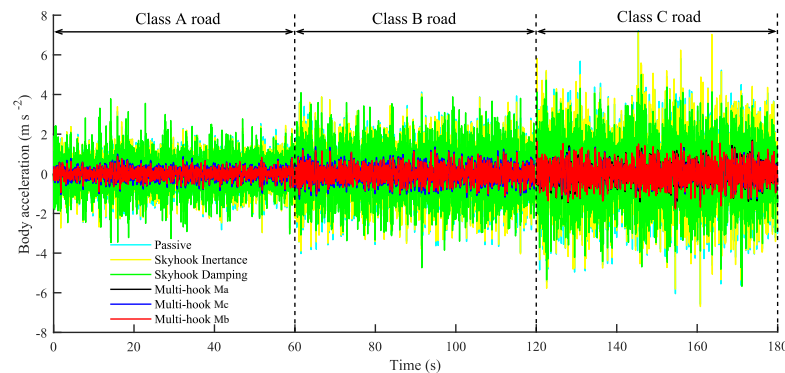


**Figure 7.** Time response comparison of body acceleration for single-skyhook and multi-hook control strategies.

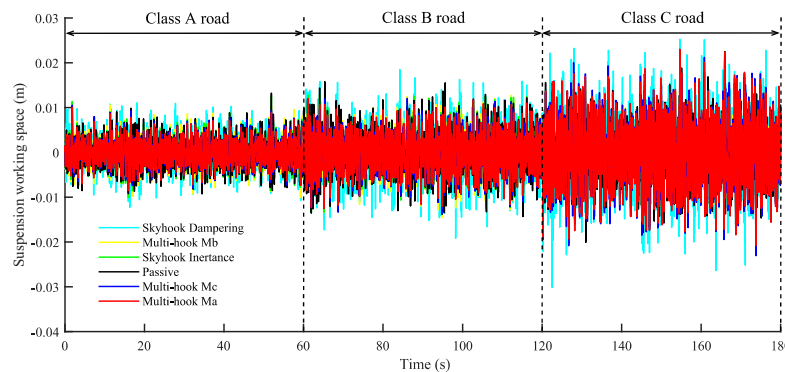


**Figure 8.** Time response comparison of suspension working space for single-skyhook and multi-hook control strategies.

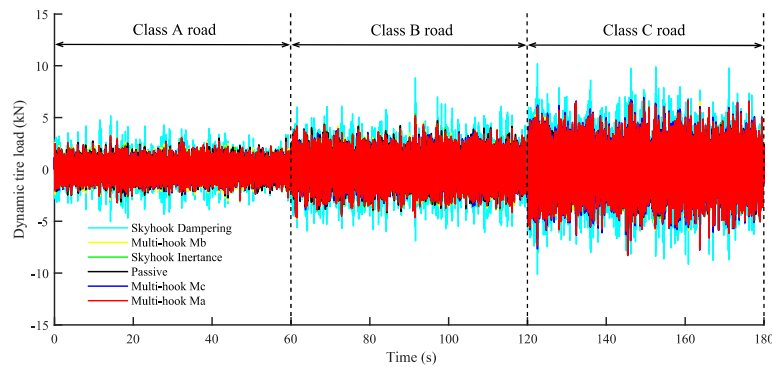


**Figure 9.** Time response comparison of dynamic tire load for single-skyhook and multi-hook control strategies.

The BA simulation results are transformed by using the FFT technique to obtain the frequency domain response, as shown in Figure 10. It can be seen that the BA of the multi-hook-controlled suspension outperforms the passive and the single-canopy suspension in the entire frequency domain from 0–15 Hz.

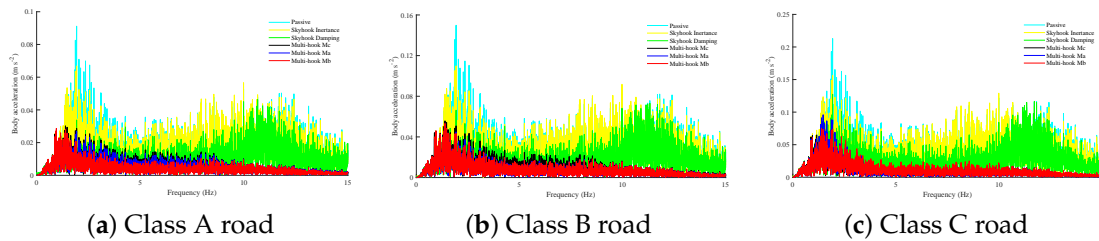


**Figure 10.** Frequency response comparison of body acceleration for single-skyhook and multi-hook control strategies.

### 4.3.2. Frequency Response Analysis

Under the same excitation given in Section 4.1.1, the RMS values of the suspension performance indicators are obtained and shown in Figure 11. The peak values in the graph are listed in Table 10.

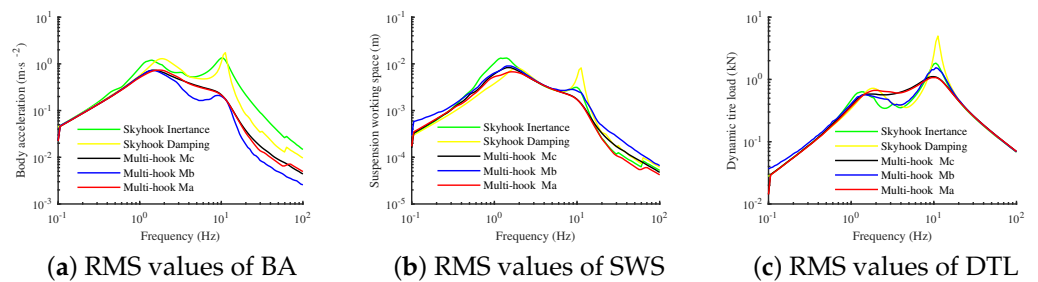


**Figure 11.** Frequency response comparison between single-skyhook and multi-hook control strategies.

According to Figure 11a, the controls with skyhook inerter, i.e., the skyhook inertance control and the multi-hook controls, have smaller natural frequencies of sprung mass than the skyhook damping control. This further verifies that the multi-hook control can simulate full-load conditions. In addition, compared with the skyhook damping control, the low-frequency peak and high-frequency peak of the other four kinds of control are reduced, as shown in Table 10.

It should be noted that in Figure 11a, multi-hook controls have smaller BA values than single-skyhook controls in the entire frequency band, meaning that the multi-hook controls are capable of obtaining the desired performance. It can be seen from Figure 11b

and Table 10 that the SWS values of multi-hook controls are between the skyhook damping and the skyhook inertance controls in the low-frequency band, while in the high-frequency band, these values are the lowest, indicating that the multi-hook controls can make full use of the suspension stroke in the low-frequency band and offer a better ride comfort in the high-frequency band.

**Table 10.** Comparison of peak RMS values for single-skyhook and multi-hook control strategies.

	Indexes	Skyhook Inertance	Skyhook Damping	Ma	Mb	Mc
BA	Low-frequency peak value ( $\text{m s}^{-2}$ )	1.20	1.29	0.74	0.72	0.73
	High-frequency peak value ( $\text{m s}^{-2}$ )	1.34	1.74	0.21	0.21	0.22
SWS	Low-frequency peak value (m)	0.0132	0.0081	0.0067	0.0090	0.0083
	High-frequency peak value (m)	0.0031	0.0082	0.0019	0.0028	0.019
DTL	Low-frequency peak value (kN)	0.63	0.72	0.67	0.57	0.57
	High-frequency peak value (kN)	1.83	4.99	1.07	1.54	1.10

Figure 11c and Table 10 show that the low-frequency peak of Ma is slightly higher than that of the skyhook inertance, but overall, the low- and high-frequency peaks of the multi-hook controls are lower than those of the single-skyhook controls, which is because the introduction of the groundhook damper directly suppresses the vertical vibration of the wheel. In summary, compared with single-skyhook controls, the multi-hook controls can achieve better ride comfort and road holding because they are able to consider both of these factors comprehensively.

## 5. Conclusions

This paper proposes an ideal multi-hook system combining skyhook inertance and skyhook damping, which addresses one limitation of the single-skyhook damping or skyhook inertance control strategies, i.e., they cannot simultaneously adapt to variations in both road and load conditions. The proposed system is able to strike a balance between smoothness and tire grounding. Three different control strategies are used to semi-actively realize the ideal multi-hook system, namely independent, inertance-based and damping-based control, which are investigated through simulation. The results show that:

1. Compared with passive suspensions, semi-active suspensions with a multi-hook control strategy experience less variation in the resonant frequency of the sprung mass when load conditions change, especially for multi-hook Mb and multi-hook Mc. In addition, multi-hook-controlled suspensions also have lower RMS values of body acceleration and are less likely to be influenced by load changes compared with passive suspensions. The multi-hook control, therefore, has superior load adaptability.
2. As road conditions change, the semi-active suspension with multi-hook control shows a significant reduction in body acceleration for all road conditions compared with the passive suspension, especially for multi-hook controls Mb and Mc, and the range of variation in the RMS value of body acceleration is lower than that of the passive suspension. Therefore, the multi-hook control is road-adaptive.
3. Compared with the single skyhook control strategy, the multi-hook control strategy allows the vehicle to achieve good ride smoothness while fully considering the need for tire grounding. This is because the introduction of groundhook damping effectively suppresses vertical tire vibrations. To summarize, multi-hook control strategy, which combines a skyhook inerter and multi-hook damper, offers both load and road adaptation and better balances smoothness and safety.

**Author Contributions:** Conceptualization, X.Z., Y.Z. (Yimu Zhang) and Y.Z. (Yue Zhao); methodology, X.Z.; software, Y.Z. (Yimu Zhang) and Y.Z. (Yue Zhao); validation, X.Z., Y.Z. (Yimu Zhang), Y.Z. (Yue Zhao) and J.N.; formal analysis, X.Z.; investigation, J.N.; resources, X.Z.; data curation, X.Z.; writing—original draft preparation, X.Z.; writing—review and editing, X.Z.; project administration, X.Z.; funding acquisition, X.Z. All authors have read and agreed to the published version of the manuscript.

**Funding:** This research was funded by the National Natural Science Foundation of China, grant number 51875257.

**Institutional Review Board Statement:** Not applicable.

**Informed Consent Statement:** Not applicable.

**Data Availability Statement:** Data sharing not applicable.

**Acknowledgments:** The authors are grateful to the editor and anonymous reviewers for their constructive comments and suggestions which have improved this paper.

**Conflicts of Interest:** The authors declare no conflict of interest.

## References

- Kim, J.G.; Yoon, Y.S. Systematic development of vehicle suspensions having passive DOF and/or redundant constraint. *Int. J. Veh. Des.* **2005**, *38*, 275–289. [\[CrossRef\]](#)
- Smith, M.C.; Swift, S.J. Design of passive vehicle suspensions for maximal least damping ratio. *Veh. Syst. Dyn.* **2016**, *54*, 568–584. [\[CrossRef\]](#)
- Issa, M.; Samn, A. Passive vehicle suspension system optimization using Harris Hawk Optimization algorithm. *Math. Comput. Simul.* **2022**, *191*, 328–345. [\[CrossRef\]](#)
- Sun, W.; Li, Y.; Huang, J.; Zhang, N. Efficiency improvement of vehicle active suspension based on multi-objective integrated optimization. *J. Vib. Control.* **2017**, *23*, 539–554. [\[CrossRef\]](#)
- Li, Z.; Zheng, L.; Ren, Y.; Li, Y.; Xiong, Z. Multi-objective optimization of active suspension system in electric vehicle with in-wheel-motor against the negative electromechanical coupling effects. *Mech. Syst. Signal Process.* **2019**, *116*, 545–565. [\[CrossRef\]](#)
- Meng, Q.; Qian, C.; Sun, Z.Y.; Chen, C.C. A homogeneous domination output feedback control method for active suspension of intelligent electric vehicle. *Nonlinear Dyn.* **2021**, *103*, 1627–1644. [\[CrossRef\]](#)
- Yang, J.; Ning, D.; Sun, S.S.; Zheng, J.; Lu, H.; Nakano, M.; Zhang, S.; Du, H.; Li, W.H. A semi-active suspension using a magnetorheological damper with nonlinear negative-stiffness component. *Mech. Syst. Signal Process.* **2021**, *147*, 107071. [\[CrossRef\]](#)
- Basargan, H.; Mihály, A.; Gáspár, P.; Sename, O. An lpv-based online reconfigurable adaptive semi-active suspension control with mr damper. *Energies* **2022**, *15*, 3648. [\[CrossRef\]](#)
- Karnopp, D.; Crosby, M.; Harwood, A. Vibration control using semi-active force generators. *J. Eng. Ind.* **1974**, *96*, 619–626. [\[CrossRef\]](#)
- Du, X.; Yu, M.; Fu, J.; Huang, C. Experimental study on shock control of a vehicle semi-active suspension with magneto-rheological damper. *Smart Mater. Struct.* **2020**, *29*, 074002. [\[CrossRef\]](#)
- Ma, T.; Bi, F.; Wang, X.; Tian, C.; Lin, J.; Wang, J.; Pang, G. Optimized fuzzy skyhook control for semi-active vehicle suspension with new inverse model of magnetorheological fluid damper. *Energies* **2021**, *14*, 1674. [\[CrossRef\]](#)
- Ahmadian, M.; Vahdati, N. Transient dynamics of semiactive suspensions with hybrid control. *J. Intell. Mater. Syst. Struct.* **2006**, *17*, 145–153. [\[CrossRef\]](#)
- Smith, M. Synthesis of mechanical networks: the inerter. *IEEE Trans. Autom. Control* **2002**, *47*, 1648–1662. [\[CrossRef\]](#)
- Li, F.; Li, X.; Shang, D.; Wang, Z. Dynamic modeling and damping performance improvement of two stage isd suspension system. *Proc. Inst. Mech. Eng. Part D J. Automob. Eng.* **2022**, *236*, 2259–2271. [\[CrossRef\]](#)
- Shen, Y.; Chen, L.; Yang, X.; Shi, D.; Yang, J. Improved design of dynamic vibration absorber by using the inerter and its application in vehicle suspension. *J. Sound Vib.* **2016**, *361*, 148–158. [\[CrossRef\]](#)
- Wang, R.; Ye, Q.; Sun, Z.; Zhou, W.; Cao, Y.; Chen, L. A study of the hydraulically interconnected inerter-spring-damper suspension system. *Mech. Based Des. Struct. Mach.* **2017**, *45*, 415–429. [\[CrossRef\]](#)
- Nie, J.; Yang, Y.; Jiang, T.; Zhang, H. Passive skyhook suspension reduction for improvement of ride comfort in an off-road vehicle. *IEEE Access* **2019**, *7*, 150710–150719. [\[CrossRef\]](#)
- Scheibe, F.; Smith, M.C. Analytical solutions for optimal ride comfort and tyre grip for passive vehicle suspensions. *Veh. Syst. Dyn.* **2009**, *47*, 1229–1252. [\[CrossRef\]](#)
- Alexey, K.; Musa, M. Optimization of improved suspension system with inerter device of the quarter-car model in vibration analysis. *Arch. Appl. Mech.* **2011**, *81*, 1427–1437.
- Hu, Y.; Chen, M.Z.; Shu, Z. Passive vehicle suspensions employing inerters with multiple performance requirements. *J. Sound Vib.* **2014**, *333*, 2212–2225. [\[CrossRef\]](#)

21. Chen, M.Z.; Hu, Y.; Li, C.; Chen, G. Semi-active suspension with semi-active inerter and semi-active damper. *IFAC Proc. Vol.* **2014**, *47*, 11225–11230. [[CrossRef](#)]
22. Chen, M.Z.; Hu, Y.; Li, C.; Chen, G. Application of semi-active inerter in semi-active suspensions via force tracking. *J. Vib. Acoust.* **2016**, *138*, 041014.1–041014.11. [[CrossRef](#)]
23. Wang, Y.; Ding, H.; Chen, L.Q. Averaging analysis on a semi-active inerter-based suspension system with relative-acceleration–relative-velocity control. *J. Vib. Control* **2020**, *26*, 1199–1215. [[CrossRef](#)]
24. Hu, Y.; Chen, M.Z.; Sun, Y. Comfort-oriented vehicle suspension design with skyhook inerter configuration. *J. Sound Vib.* **2017**, *405*, 34–47. [[CrossRef](#)]
25. Zhang, X.L.; Zhu, J.; Nie, J.; Gene Liao, Y.; Lu, X. Analysis of inertance and damping double-skyhook control strategies for a semi-active device combining an adjustable inerter and damper. *Struct. Control Health Monit.* **2022**, *29*, e3040. [[CrossRef](#)]
26. Valášek, M.; Novak, M.; Šika, Z.; Vaculin, O. Extended ground-hook-new concept of semi-active control of truck's suspension. *Veh. Syst. Dyn.* **1997**, *27*, 289–303. [[CrossRef](#)]
27. Zhao, L.; Yu, Y.; Zhou, C.; Li, X.L. Analytical matching of optimal damping characteristics curve for vehicle passive suspensions. *Int. J. Eng.* **2018**, *31*, 2109–2114.
28. Zhao, L.; Zhou, C.; Yu, Y. A research on optimal damping ratio control strategy for semi-active suspension system. *Automot. Eng.* **2018**, *40*, 41–47.